Remediation Ecology
https://www.sciltp.com/journals/re

Article

Adsorptive Removal of Zn(II) from Aqueous Solution Using Fermented Sweet Sorghum Stalk Residues Grafted with Acrylic Acid by Irradiation

Jinling Wu [1,2,*], Jing Dong [1] and Xuan Guo [1]

[1] Laboratory of Environmental Technology, INET, Tsinghua University, Beijing 100084, China
[2] CAEA Center of Excellence on Nuclear Technology Applications for Electron Beam on Environmental Application, Tsinghua University, Beijing 100084, China
* Correspondence: jinlingwu@tsinghua.edu.cn; Tel.: +86-10-6279-6856

How To Cite: Wu, J.; Dong, J.; Guo, X. Adsorptive Removal of Zn(II) from Aqueous Solution Using Fermented Sweet Sorghum Stalk Residues Grafted with Acrylic Acid by Irradiation. *Remediation Ecology* **2026**, *1*(1), 4.

Received: 19 March 2026
Revised: 17 April 2026
Accepted: 22 May 2026
Published: 4 June 2026

Abstract: A novel biosorbent was prepared by grafting acrylic acid (AAc) onto fermented sweet sorghum stalk residues (FSSR) via γ-ray radiation for the adsorptive removal of Zn(II) from aqueous solution. FSSR is a typical by-product of bioethanol production, enabling low-cost and sustainable wastewater treatment. To reveal the interfacial interaction mechanism between Zn(II) and the grafted FSSR adsorbent, the Zn species, key surface functional groups, and coordination structure were systematically investigated using X-ray absorption spectroscopy techniques. Results demonstrated that γ-ray radiation effectively introduced abundant carboxyl groups onto FSSR, significantly enhancing its Zn(II) adsorption performance. Extended X-ray Absorption Fine Structure (EXAFS) analysis confirmed that Zn(II) was adsorbed as divalent cations mainly through carboxyl coordination. The coordination number N was 4.2 and a Zn-O atomic distance was approximately 1.93 Å. This work provides a promising strategy for the valorization of agricultural residues and the rational design of high-efficiency biosorbents for heavy metal contaminated water remediation.

Keywords: Zinc; biosorbent; grafting; fermented sweet sorghum stalk residues (FSSR); EXAFS

1. Introduction

Heavy metals that pollute the environment include lead, cadmium, mercury, arsenic with significant biological toxicity, as well as copper, cobalt, zinc and other heavy metal pollutants. These metals are essential trace elements for living organisms but can still cause adverse ecological effects at excessive levels [1,2]. Zn(II) is a micronutrient for plants and animals at low concentrations, but it is toxic at high concentrations [3]. Zn(II) persists in the environment and is non-biodegradable. Even at trace levels, it can cause chronic damage to human organs through bioaccumulation along the food chain. The main sources of Zn(II) in the environment are anthropogenic activities, including mining and smelting of metal ores [4], electroplating, waste gas emission, energy and fuel production, urban garbage generation, pesticides and sewage sludge, and agricultural land. The research and development of the effective and economical method for heavy metal separation in wastewater treatment has attracted increasing attention with the rapid development of environmental technology [5].

Adsorption is widely regarded as a promising technique owing to its simplicity and efficiency, in which the selection and design of adsorbents play a decisive role [6,7]. In recent years, agricultural and forestry wastes have been increasingly explored as low-cost biosorbents for heavy metal removal from aqueous solutions [8–16]. A variety of biomass-based materials have been studied, including lignocellulosic waste [9], hemicellulose [17], loofah [18], leaf [19], rice husk [20], chitosan [21] and straw [22]. Such wastes are abundant, diverse, and often

Copyright: © 2026 by the authors. This is an open access article under the terms and conditions of the Creative Commons Attribution (CC BY) license (https://creativecommons.org/licenses/by/4.0/).
Publisher's Note: Scilight stays neutral with regard to jurisdictional claims in published maps and institutional affiliations.

discarded in large quantities, leading to land occupation and potential pollution of soil and groundwater. Recycling these residues as biosorbents for Zn(II) and other heavy metals enables their secondary utilization and brings additional environmental benefits.

However, despite their obvious advantages such as low cost, biodegradability, ready availability, and operational simplicity, raw agricultural and forestry wastes generally suffer from critical drawbacks, including low adsorption capacity, insufficient active sites, poor selectivity toward target heavy metals, and low surface reactivity. These limitations severely restrict their practical application in real wastewater treatment. To overcome these bottlenecks, chemical modification has been widely employed to enhance the adsorption performance of biomass toward Zn(II). For instance, Bhadoria et al. modified rice straw to prepare three bio-adsorbents, but the optimal Zn(II) removal efficiency was only 8.4% [23]. Karimi et al. developed a modified chitosan adsorbent Zn with the removal degree of 83.81% [24]. Dudziak et al. prepared biochars from the waste straw and sewage sludge for Zn(II) adsorption, yet the maximum adsorption capacity was merely 2 mg/g [25]. These results indicate that although conventional modification methods can improve performance to a certain extent, issues such as low capacity, complex synthesis, and limited scalability still remain largely unsolved.

Against this background, radiation-induced grafting has emerged as an innovative and efficient strategy for adsorbent preparation. Gamma irradiation can generate active free radicals on the biomass substrate and initiate graft copolymerization with functional monomers, thereby introducing abundant chelating groups in a controllable and environmentally friendly manner [26]. Notably, indirect irradiation allows the separation of the irradiation and grafting steps, which is favorable for large-scale production. To date, radiation grafting has been successfully applied to develop high-performance adsorbents for various heavy metals. Tang et al. used electron beam-induced grafting of calix [4] arene and achieved a Cu(II) adsorption capacity of 123.3 mg/g [27]. He et al. prepared four irradiation-functionalized adsorbents for uranium removal from high-salinity water [28]. Torkaman and Asadollahzadel grafted glycidyl methacrylate onto polypropylene non-woven fibers via gamma radiation, followed by amination and phosphorylation for La(III) adsorption [29]. Misra et al. modified cotton cellulose with bis(2-methacryloxyethyl) phosphate using gamma radiation for U(IV) removal from groundwater [30]. Selambakkannu et al. functionalized PP/PE non-woven fabrics with 2-dimethylaminoethyl methacrylate via electron beam irradiation for thorium adsorption [31]. Dong et al. grafted acrylic acid onto sweet sorghum stalks using γ-rays, introducing approximately 1.6 mmol/g carboxyl groups and achieving a Cu(II) adsorption capacity of 13.32 mg/g [32]. Despite these advances, few studies have focused on the rational design of grafted biosorbents specifically for Zn(II) removal, and the interfacial coordination mechanism remains poorly understood at the molecular level.

Advanced spectroscopic techniques are essential for revealing the micro-interactions between heavy metals and adsorbent surfaces, including FTIR, XPS, ESR, EXAFS, and XANES. Among them, EXAFS provides detailed information on the local coordination environment of metal ions, such as valence state, identity of coordinating atoms, and bond distances, enabling in-depth mechanistic analysis [33,34]. Combined with surface complexation models, EXAFS can elucidate the true adsorption mechanism [35–38]. XANES is complementary to EXAFS and can sensitively reflect changes in the valence state and coordination geometry of the target metal. For example, Zhu et al. and Ledingham et al. determined Zn speciation in soils and minerals using Zn K-edge XANES [39,40]. Dupont et al. used lignocellulosic biosorbents for Cu(II) and Pb(II) removal and identified a six-coordinate structure for Cu(II) with equatorial and axial oxygen ligands via X-ray absorption spectroscopy [41]. Their results confirmed that Cu and Pb bind primarily to carboxylic groups on lignocellulose.

In this study, a novel biosorbent was synthesized by grafting acrylic acid (AAc) onto fermented sweet sorghum stalk residue (FSSR) via γ-ray irradiation, and its adsorption performance toward Zn(II) was systematically investigated. To gain molecular-level insight into the interfacial interaction between Zn(II) and the grafted FSSR adsorbent, XANES and EXAFS were employed to identify Zn(II) speciation, key surface functional groups, and the coordination structure between Zn(II) and active sites. This work not only provides a high-efficiency, low-cost biosorbent for Zn(II) wastewater treatment but also clarifies its adsorption mechanism at the atomic scale, thereby supporting the rational design of advanced biomass-based adsorbents for heavy metal remediation.

2. Materials and Methods

2.1. Preparation of FSSR and FSSR-AAc

The original FSSR was obtained from solid-state fermentation of sweet sorghum stalk for the production of ethanol, and the optimal grafting conditions were according to our previous study [32]. Under this condition, the grafting rate reached 10.2%. This study adopted this condition. A certain mass of FSSR was added into 10 times the mass of N, N-Dimethylacetamide (DMAC) and soaked at 100 °C for 3 h. The swelled FSSR was filtered and

10% acrylic acid was added, then a certain amount of sodium hydroxide was added to the neutralization degree of 0.6 after cooled to room temperature. Nitrogen gas was added into the FSSR for 15 min. After standing overnight the grafted products were irradiated by Co-60 gamma ray at 10 kGy. The irradiated products were washed with hot water at 100 °C for 6 h. The grafted products were filtered out and dried at 70 °C and then ground to obtain FSSR-AAc.

2.2. Chemical Reagents

NaOH, H_2SO_4, HCl were analytical reagents obtained from Beijing Chemical Plant (China). $ZnCl_2 \cdot 7H_2O$ was an analytical reagent obtained from Sinopharm Chemical Reagent Company (China).

2.3. Adsorption Experiment

$ZnCl_2$ solution (50 mg/L) was adjusted to initial pH of 5.0 by HCl, then 0.1 g of FSSR or FSSR-AAc was added. The solution was shaken at 150 rpm at 30 °C for 4 h. Different conditions were applied, including initial Zn(II) concentration (25–250 mg/L), temperature (283.15–313.15 K). The experiments were performed three times for each condition.

$$q_e = \frac{C_0 - C_e}{W} V \tag{1}$$

Equation (1) is the expression of adsorption capacity q_e which is Zn(II) adsorption capacity (mg/g); C_o is the initial concentration of Zn(II) (mg/L); C_e is the equilibrium concentration of Zn(II) (mg/L); W is the mass of biosorbent (g); V is the volume of solution (L).

2.4. Analysis of Zn(II) Concentration

The concentrations of Zn(II) were determined by atomic absorption spectrophotometer (Jena Vario 6, Jena, Germany).

2.5. Characterization of Original FSSR and FSSR-AAc

FSSR and FSSR-AAc were characterized and analyzed by SEM (Fei Quanta 200FEG field scanning electronic microscope, Eindhoven, The Netherlands) and XRD (D/max TTR III X-ray diffractometer, Hokuto, Yamanashi, Japan) with the range of 2θ of 7.5–90°.

The carboxyl concentration of materials was determined by titration: 0.1 g of grafted samples were treated with 0.01 mol/L excess NaOH. 25 mL of filtrate was titrated with 0.01 mol/L HCl. The Equation (2) expresses the carboxyl concentration:

$$C_{-COOH} = \frac{C_{NaOH} V_{NaOH} - 4 C_{HCl} V_{HCl}}{m} \tag{2}$$

In Equation (2), $C_{\text{-}COOH}$ is carboxyl concentration (mmol/L); C_{NaOH} is NaOH concentration (mmol/L), C_{HCl} is HCl concentration (mmol/L), V_{NaOH} is the NaOH solution volume (L), V_{HCl} is the HCl solution volume (L), m is the sample mass (g).

2.6. Analysis of Interaction between Zn(II) and FSSR-AAc

The FSSR-AAc after Zn(II) adsorption was sampled, ground into powder, sieved through 400 mesh, and then coated with adhesive tape for XANES determination. Typical metal anion Zn (II) reference materials were ZnO, $Zn(NO_3)_2$, $ZnSO_4$ and $Zn(CH_3COO)_2$. The XANES experiment was carried out through the synchrotron radiation facility at the Institute of high energy physics, Chinese Academy of Sciences (Beijing, China). The reference sample was measured in transmission mode. The Zn(II) adsorbed FSSR (Zn-FSSR) sample was measured in fluorescence mode. The measurement range of the spectrum was from 200 EV before the absorption edge to 800 EV after the absorption edge. The spectrum was solved by software IFEFFIT (Interactive XAFS Analysis, Matt Newville, CARS, University of Chicago, USA, open-source software).

2.7. Adsorption Isotherm Models

In the isothermal study, the Langmuir, Freundlich, Temkin and Redlich-Peterson models were applied [42].

3. Results and Discussion

3.1. Adsorption of Zn(II) by Original FSSR and FSSR-AAc

The Zn(II) adsorption isotherms of FSSR and FSSR-AAc are presented in Figures 1a,b and 2, with corresponding fitting parameters summarized in Tables 1 and 2. Similar to the Cu(II) adsorption behavior of FSSR reported previously [13], the adsorption capacity of both samples increased slightly with rising temperature.

Table 1. The parameters of isotherm models for Zn(II) adsorption by original FSSR.

Model	Temperature (K)			
	283.15	**293.15**	**303.15**	**313.15**
Langmuir				
q_m(mg/g)	1.20 ± 0.19	2.43 ± 0.21	2.48 ± 0.19	2.75 ± 0.16
K_L(L/mg)	0.047 ± 0.021	0.036 ± 0.013	0.046 ± 0.016	0.064 ± 0.020
R^2	0.950	0.939	0.926	0.940
Freundlich				
K_F(mg/g)	0.517 ± 0.096	0.494 ± 0.081	0.600 ± 0.090	0.811 ± 0.099
n	4.13 ± 0.67	3.53 ± 0.43	3.91 ± 0.48	4.45 ± 0.51
R^2	0.979	0.983	0.971	0.985
Temkin				
A (L/g)	1.03 ± 0.96	0.65 ± 0.42	0.99 ± 0.67	1.81 ± 1.35
B (J/mol)	2962 ± 610	2382 ± 375	2539 ± 405	2540 ± 379
R^2	0.891	0.894	0.851	0.895

Table 2. The parameters of isotherm models for Zn(II) adsorption by FSSR-AAc.

Model	Temperature (K)			
	283.15	**293.15**	**303.15**	**313.15**
Langmuir				
q_m(mg/g)	16.1 ± 1.1	17.4 ± 1.0	20.1 ± 1.2	21.0 ± 1.1
K_L(L/mg)	0.115 ± 0.031	0.163 ± 0.042	0.121 ± 0.026	0.143 ± 0.028
R^2	0.970	0.959	0.962	0.975
Freundlich				
K_F(mg/g)	4.33 ± 1.23	5.44 ± 1.23	5.33 ± 1.16	5.72 ± 1.14
n	3.70 ± 0.96	4.06 ± 0.95	3.60 ± 0.74	3.59 ± 0.68
R^2	0.917	0.902	0.878	0.896
Temkin				
A (L/g)	1.60 ± 1.00	2.96 ± 1.82	1.65 ± 0.76	1.87 ± 0.80
B (J/mol)	343 ± 57	355 ± 53	292 ± 38	287 ± 35
R^2	0.925	0.909	0.895	0.922

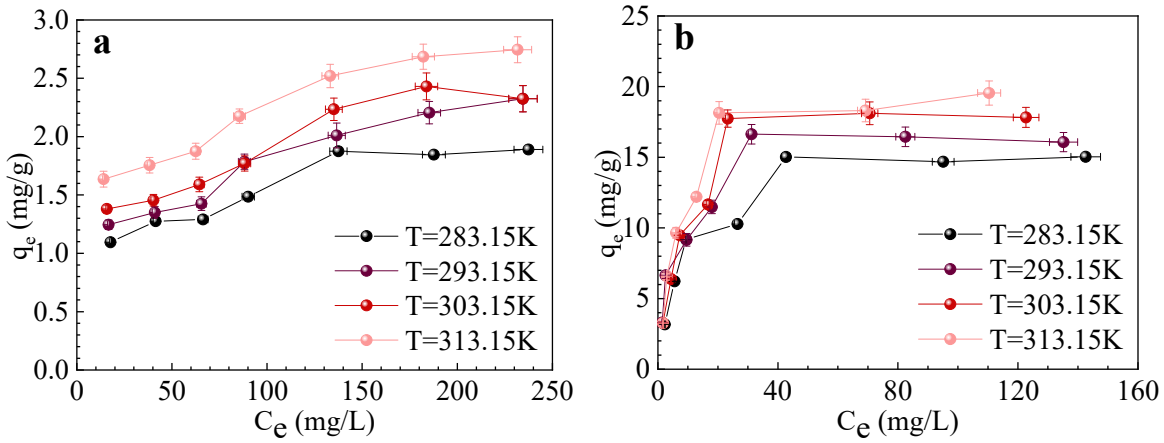

Figure 1. Langmuir isothermal adsorption model fitting curves: (**a**) FSSR; (**b**) FSSR/AAc.

For unmodified FSSR, the Freundlich model provided the best fitting performance with a correlation coefficient R^2 above 0.97, followed by the Langmuir model with $R^2 > 0.93$. The fitted values of *n* in the Freundlich model ranged from 3.5 to 4.5, indicating favorable adsorption conditions.

For FSSR-AAc, the adsorption data were best described by the Langmuir isotherm model. The maximum adsorption capacity reached 20.98 mg/g at 313.15 K, which was more than six times higher than that of raw FSSR (2.75 mg/g).

The Redlich-Peterson model failed to provide satisfactory fitting for both adsorbents, and thus corresponding parameters are not listed in Tables 1 and 2.

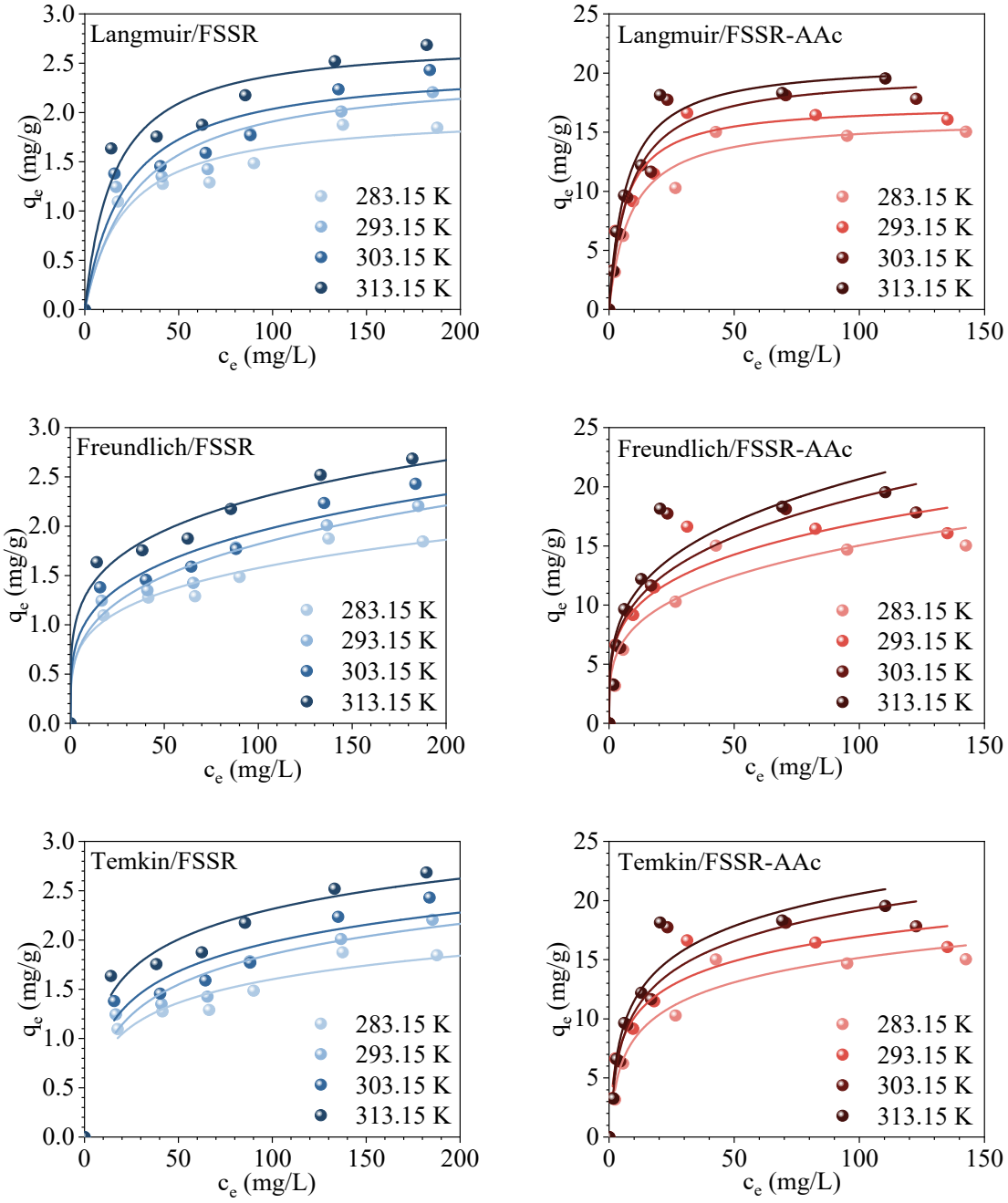

Figure 2. Adsorption isotherm modelling for Zn(II) by FSSR and FSSR-AAc.

3.2. Characterization of FSSR and FSSR-AAc

FSSR was grafted under the optimized grafting conditions. The monomer concentration was 10% and the irradiation dose was 10 kGy. The grafted materials were characterized by scanning electron microscope, FTIR and XRD.

3.2.1. SEM Observation

FSSR and FSSR-AAc surface morphology was observed by the SEM, which were shown in Figure 3. FSSR had a rough and uneven surface which contained a large number of micropores. Compared with FSSR, the surface

morphology of grafted FSSR-AAc had no obvious change. The surface of grafted material was slightly rougher and irregular.

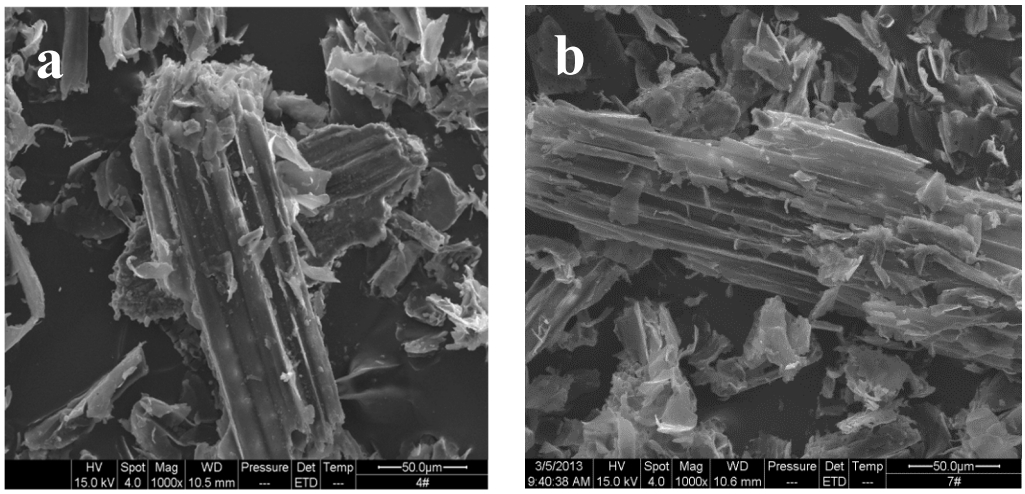

Figure 3. The SEM images of original FSSR (**a**) and FSSR-AAc (**b**).

3.2.2. XRD

The XRD patterns of FSSR were shown in Figure 4, the diffraction peaks of 15.5° and 22.5° corresponded to the amorphous region and crystalline region of cellulose, respectively. FSSR have obvious crystalline structure and amorphous region due to the existence of cellulose.

Equation (3) can be used to calculate the crystallinity (CRI), which evaluates cellulose crystal structure [43].

$$CrI = \left(\frac{I_{002} - I_{am}}{I_{002}} \right) \times 100\% = \left(1 - \frac{I_{am}}{I_{002}} \right) \times 100\% \quad (3)$$

where I_{002} is the maximal diffraction peak with 2 θ of 22~23° (cellulose I; 18~22° for cellulose II); I_{am} is the maximal diffraction peak with 2 θ of 18~19° (cellulose I; 13~15° for cellulose II). For natural lignocellulosic materials, it usually refers to cellulose I.

According to the calculation (Table 3), the crystallinity (CRI) of original FSSR and FSSR-AAc were 47% and 35% respectively, indicating that grafting destroyed crystalline cellulose. Compared with original FSSR, the crystallinity of the grafted FSSR-AAc decreased significantly.

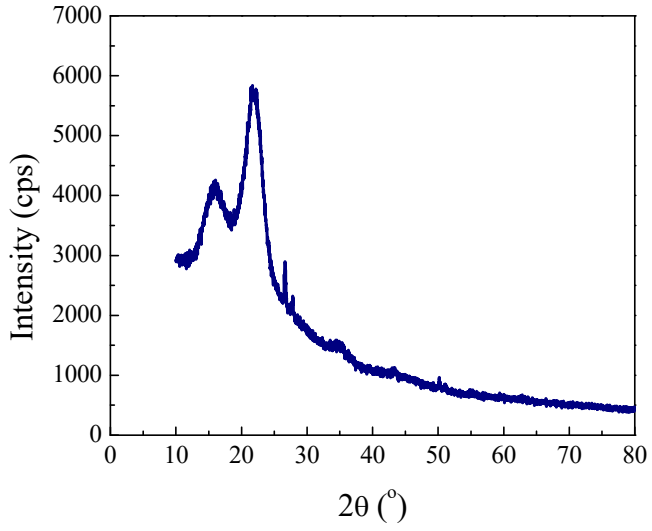

Figure 4. XRD spectrum of FSSR.

Table 3. Crystallinity of FSSR and FSSR-AAc.

Biosorbent	Crystallinity
FSSR	47 ± 2%
FSSR-AAc	35 ± 2%

3.2.3. Carboxyl Functional Group Analysis

The contents of carboxyl functional groups of original FSSR and FSSR-AAc before and after grafting were determined. The contents of carboxyl functional group in FSSR and FSSR-AAc were 0.20 ± 0.05 and 1.60 ± 0.07 mmol/g. Carboxyl functional groups increased on the surface of FSSR after grafting.

FTIR results also proved acrylic acid had been successfully grafted onto FSSR surface. The results could refer to our previous publication [32].

3.3. XANES Spectra

3.3.1. K Spatial Curves

The k-space curve represents the local structure of substances in EXAFS. Different curves indicate the difference of local structure of substances (Figure 5a). By analyzing the spectrum with K^3 weight, the absorption spectrum at larger wavelength can be balanced. The k-space curves of FSSR-AAc-Zn(II) were compared with the reference materials of $Zn(CH_3COO)_2$, ZnO and Zn $(NO_3)_2$, as shown in Figure 5b–d. The k-space curve of FSSR-AAc-Zn(II) was significantly different from those of ZnO and $Zn(NO_3)_2$, which indicated that the local structure of Zn(II) adsorbed by FSSR-AAc was significantly different from those of ZnO and $Zn(NO_3)_2$. The local structure of the bonding part between Zn(II) and FSSR-AAc was similar to that of $Zn(CH_3COO)_2$ except for the different amplitude and the shifted peak position. Because the FSSR-AAc was mixture with complex composition, its coordination environment was complex, which was difficult to be completely consistent with the k-space curve of a pure material. The k-space curve of Zn(II)-FSSR-AAc was in good agreement with that of $Zn(CH_3COO)_2$.

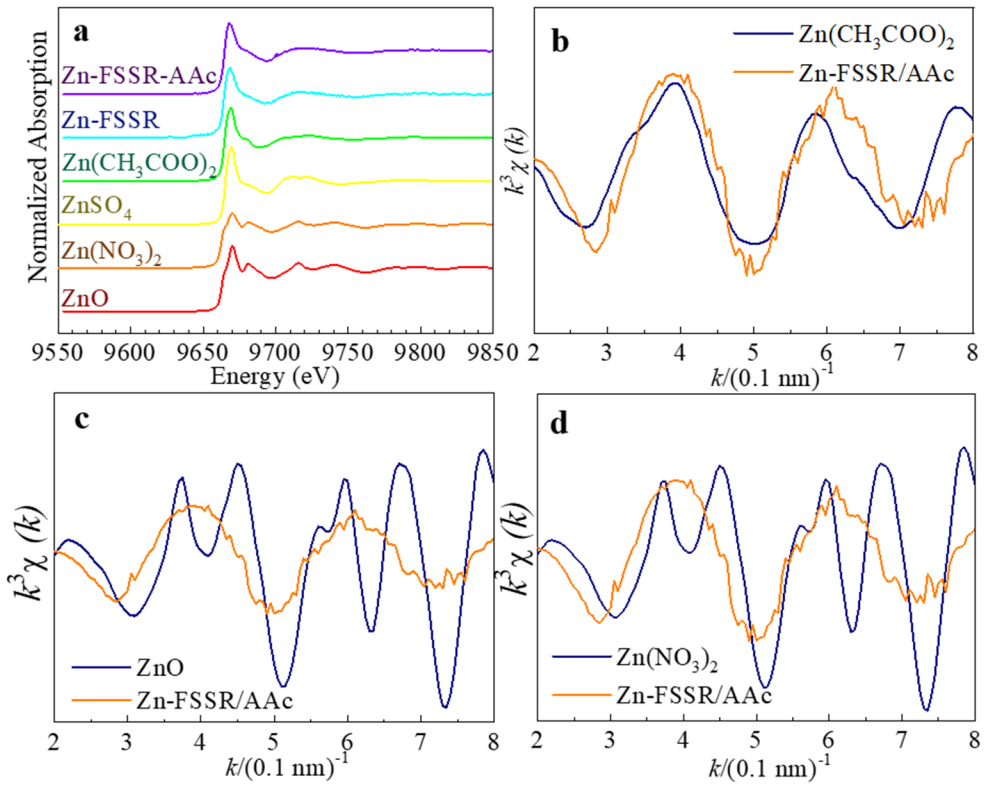

Figure 5. XANES spectra (**a**) and EXAFS spectrum (k^3 weight) of Zn-K edge for Zn-FSSR/AAc and $Zn(CH_3COO)_2$ (**b**), ZnO (**c**) and $Zn(NO_3)_2$ (**d**).

3.3.2. Radial Structure Function

The comparison of the radial structure function between Zn(II)-FSSR-AAc and the reference was shown in Figure 6. The structure function curve of Zn(II)-FSSR-AAc was closest to that of $Zn(CH_3COO)_2$ in shape. The

spectrum was significantly different from those of ZnO, $Zn(NO_3)_2$ and $ZnSO_4$. The first coordination layer in FSSR-AAc coordinated with Zn(II) is O atom. Although the first coordination layer coordinated with Zn(II) in the reference ZnO, $Zn(NO_3)_2$ and $ZnSO_4$ was O atom as well, the coordination radius and the structure were different. The main peak of FSSR-AAc-Zn was near 1.93 Å. The structure of its high coordination layer was also similar to that of $Zn(CH_3COO)_2$. The various surface functional groups were complex with its radial structure function spectrum significantly different from several reference materials such as ZnO, $Zn(NO_3)_2$, $ZnSO_4$ and $Zn(CH_3COO)_2$.

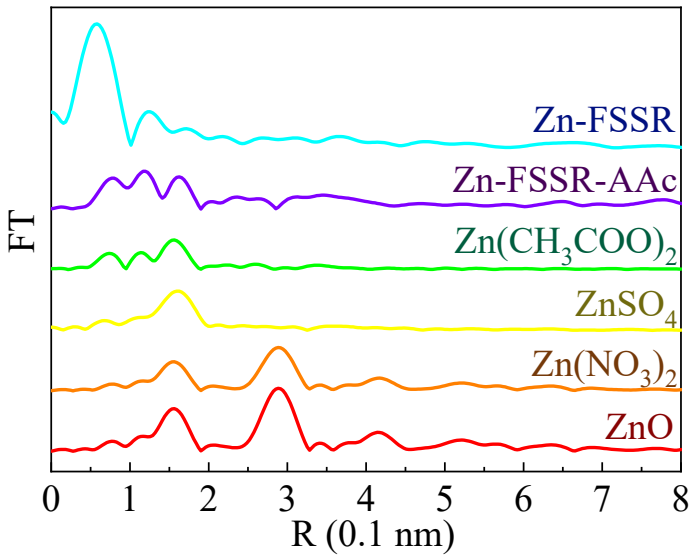

Figure 6. Radial structure function of EXAFS spectrum for ZnO, $Zn(NO_3)_2$, $ZnSO_4$, $Zn(CH_3COO)_2$, Zn-FSSR-AAc and Zn-FSSR.

3.3.3. The First Coordination Layer (Zn-O)

Taking ZnO and $Zn(CH_3COO)_2$ as references, the samples Zn-FSSR-AAc were fitted. The fitting curves are shown in Figure 7a,b respectively. Compared with the actual measured K^3 curve, the fitting effect of zinc acetate ($Zn(CH_3COO)_2$) was still the best, although the peak position and amplitude had a certain offset. Fitting obtained the coordination number of the first coordination layer of N, atomic distance of R and Debye-Waller factor of σ^2, which was listed in Table 4. The parameters of reference substances reported in the literature and the interaction parameters between some substances and Zn(II) are listed and compared.

Table 4. Fitting parameters of the first coordination layer of EXAFS sample.

Sample	Structure	Structural Parameters of the First Coordination Layer			References
		N	R	σ^2	
Zn-FSSR/AAc	Zn-O	4.232	1.93184	0.01678	This study
ZnO	Zn-O	4.00	1.96	-	[44]
$Zn(NO_3)_2$	Zn-O	6.00	2.090	0.079	[45]
$ZnSO_4$	Zn-O	5.00	2.05	0.029	[46]
$Zn(CH_3COO)_2$	Zn-O	4.00	1.93	0.019	[47]
Protein-Zn	Zn-S	1.95	2.36	0.017	[46]
Cellulose- Zn	Zn-O	6.15	2.08	0.038	[46]
Cellulose- Zn	Zn-O	6.0	2.07	0.006	[48]
Hop leaves- Zn	-	2	2.03	0.0065	[49]
Hop stem-Zn	-	2	2.01	0.0048	[49]
ZnS	Zn-S	4	2.334	0.036	[45]
ZnS	Zn-S	4	2.33	0.0032	[46]
Cysteine-Zn	Zn-S	4.08	2.25	0.053	[46]
Cysteine-Zn	Zn-S	4.5	2.35	0.007	[48]
E. coli-Zn	-	5.1	1.97	0.008	[50]
Pseudomonas putida-Zn	-	6	2.02	0.005	[50]

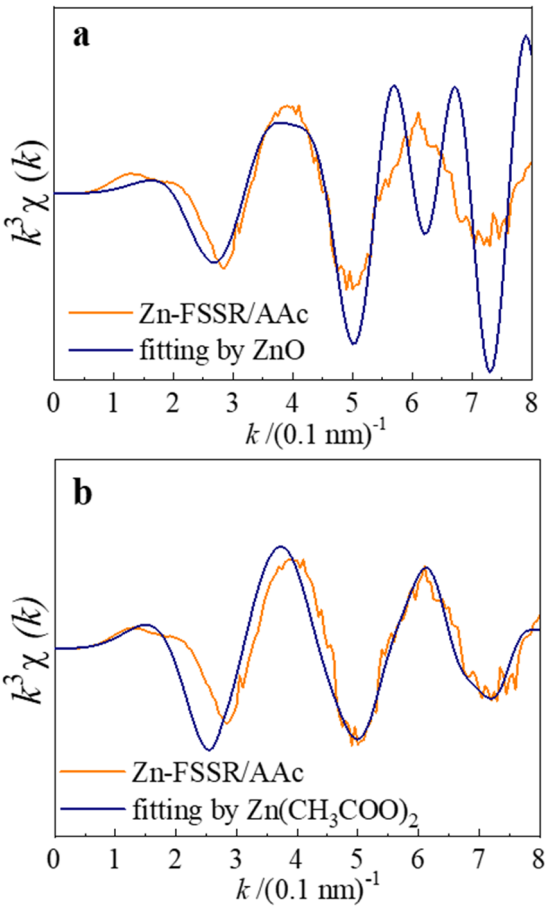

Figure 7. Fitting structure of the first coordination layer (Zn-O) of Zn-FSSR/AAc with ZnO (**a**) and $Zn(CH_3COO)_2$ (**b**) as the reference.

3.3.4. Configuration Analysis

Zn(II) is a transition metal ion with d^{10} electronic structure, that is, the outer electron has 18-electronic structure, which usually forms tetrahedral (tetra coordination) and octahedral (hexa coordination) configuration (Figure 8). The configuration is different, and the Zn-O bond length is different as well. ZnO has a typical four coordination tetrahedron configuration with the first coordination layer Zn-O bond length of 1.96 Å. The configuration of hydrated zinc ions is a typical hexa coordination octahedron configuration with the first coordination layer Zn-O bond length of 2.10 Å. The configuration of Zn(II) is usually inferred by coordination number and bond length. Therefore, the study of EXAFS can be used to determine the configuration of coordination structure with Zn(II). The reference $Zn(NO_3)_2$ reported in the literature is a hexa coordinated octahedron configuration. $Zn(CH_3COO)_2$ is a tetra coordinated tetrahedron configuration. In this study, for the grafted material FSSR-AAc adsorbing Zn(II), the coordination number N was 4.232 and the distance between Zn-O was 1.93184 Å. EXAFS analysis reveals a coordination number of 4.232 for Zn(II) adsorbed on the biomass, which is close to the tetrahedral coordination in $Zn(CH_3COO)_2$. However, considering the inherent chemical heterogeneity of biomass surfaces, a fully uniform tetrahedral coordination environment is unlikely. Instead, the value of 4.232 supports the presence of a predominantly tetrahedral coordination with minor contributions from mixed coordination modes, consistent with the complex surface chemistry of biomass materials.

Different initial pH, initial concentration and adsorption reaction temperature of adsorbate lead to different interaction configurations between the adsorption material and Zn(II). The changes of configuration can be analyzed by EXAFS. Pan et al. used EXAFS to analyze the effect of initial Zn(II) concentration on the configuration change of manganese ore after adsorption of Zn(II) [51]. With the increase of initial Zn(II) concentration from 10 to 14 mg/L, the Zn-O bond length decreased from 2.01 to 1.98 Å, and the coordination number increased from 4.0 to 4.3. Li et al. analyzed the configuration change of Zn(II) adsorbed on TiO_2 by EXAFS [52]. When the temperature increased from 5 °C to 40 °C, the Zn-O bond length decreased from 1.99 Å to 1.98 Å, and the coordination number increased from 4.3 to 4.5. Bochatay et al. Used EXAFS to analyze the influence of the initial pH of Zn(II) solution on the configuration change of Zn(II) adsorbed on manganese ore. With the increase of initial pH increased from 6.17 to 8.97, the Zn-O bond length decreased from 2.04 Å to 1.96 Å,

and the coordination number decreased from 5.9 to 4.3 [53]. The decrease of coordination number indicated that the configuration changes from octahedral configuration to tetrahedral configuration.

Due to the complex composition and structure of natural lignocellulose materials, different materials interact with Zn(II) with different coordination atoms or complex structures, so the coordination configurations are also different.

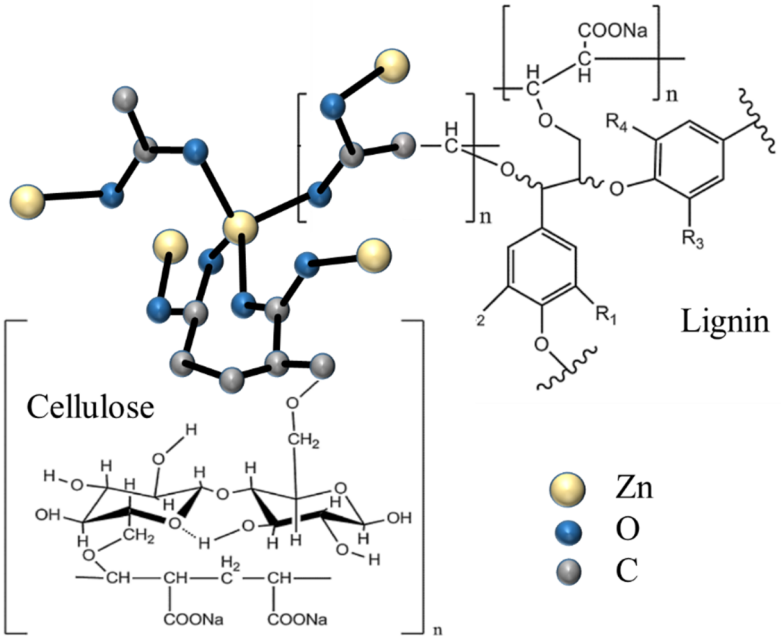

Figure 8. Proposed configuration of coordination structure of FSSR-AAc-Zn(II).

3.4. Performance Comparison and Cost-Effectiveness Analysis

3.4.1. Comparison of Zn(II) Adsorption Performance with Other Biosorbents

To further evaluate the application potential of FSSR-AAc as a biosorbent for Zn(II) removal from aqueous solution, its maximum adsorption capacity (qm) was compared with various reported biosorbents, as summarized in Table 5. The results showed that the qm of FSSR-AAc (20.98 mg/g) was significantly higher than most unmodified lignocellulosic biosorbents, such as Lantana camara leaves (2.778 mg/g), flax fibers (4.6 mg/g), and Corchorus olitorius leaves (11.63 mg/g). It was also superior to urban pruning waste (18.382 mg/g) and cross-linked carboxymethyl cellulose (10.809 mg/g). Although some biosorbents (e.g., Alhagi graecorum root and brown algae Sargassum polycystum) exhibited higher adsorption capacities, they often required complex modification processes or relied on non-waste biomass feedstocks. In contrast, FSSR-AAc was fabricated from fermented sweet sorghum stalk residues, a low-cost industrial by-product of bioethanol production, via a green and scalable γ-ray irradiation grafting method. The combination of high adsorption capacity, waste-derived feedstock, and environmentally friendly preparation endowed FSSR-AAc with distinct advantages in cost-effectiveness and sustainability for Zn(II) wastewater treatment.

Table 5. Comparison of biosorbents for Zn(II) adsorption.

Biosorbent	q_m (mg/g)	Isotherm Model	References
FSSR	2.75	Freundlich	This study
FSSR-AAc	20.98	Langmuir	This study
Urban pruning waste	18.382	Langmuir	[54]
Leaves of Corchorus olitorius	11.63	Freundlich	[55]
Fruit rind	9–39.18		[56]
Cross-linked carboxymethyl cellulose	10.809		[57]
Lantana camara leaves	2.778	Langmuir	[58]
Alhagi graecorum root	188.67	Sip	[59]
Brown algae Sargassum polycystum	116.2	Langmuir	[60]
Flax fibers	4.6 (71 mmol/kg)	Langmuir	[61]
EPS from anammox granular sludge	7.4–49.8		[62]
Chitosan from insect breeding waste	45		[63]

3.4.2. Cost-Performance of FSSR-AAc

The Zn(II) adsorption capacity of FSSR-AAc is 20.98 mg/g, which is higher than that of natural zeolite/bentonite (5–15 mg/g), equivalent to the upper limit of ordinary coal-based activated carbon (15–30 mg/g), and slightly lower than that of modified activated carbon and chelating resin. Its pilot-scale cost (80–120 yuan/kg) is lower than that of modified activated carbon (80–200 yuan/kg) and high-end commercial chelating resin (100–160 yuan/kg), showing good cost-performance.

The core advantage of FSSR-AAc lies in its sustainability: it uses FSSR, a by-product of sorghum wine production, as the base material and adopts a green γ-radiation grafting process. Its cost estimation is based on 1 kg of dry FSSR: the raw material FSSR is about 0.25 yuan, DMAC solvent (15 L, recyclable) is about 77.55 yuan, acrylic acid (0.3 kg) is about 3.9 yuan, auxiliary materials such as NaOH and nitrogen are about 1.52 yuan, energy consumption for cleaning and drying is about 10 yuan, and 10 kGy γ-radiation is about 100 yuan, totaling about 193.22 yuan/kg (dry basis). Based on an 80% yield, the small-scale finished product cost is about 241.5 yuan/kg; in the pilot-scale stage, through more than 70% DMAC recovery and ton-level radiation cost reduction, the finished product cost can be reduced to 80–120 yuan/kg, and further reduced to 60–80 yuan/kg after large-scale production. Spent adsorbents can be valorized through pyrolysis or Zn(II) recovery to avoid secondary pollution, showing good industrial application potential. This adsorbent is suitable for high-value wastewater and circular economy projects, but not for ultra-low-cost large-scale treatment scenarios.

3.4.3. Post-Use Valorization of Spent FSSR-AAc Adsorbent

The post-use valorization of the Zn(II)-loaded FSSR-AAc adsorbent is critical for realizing circular economy and minimizing secondary waste. Two feasible valorization routes are proposed for the spent biosorbent.

First, regeneration and reuse can be achieved by eluting adsorbed Zn(II) with dilute hydrochloric acid (0.1 mol/L HCl), which enables efficient desorption and recovery of Zn(II) with a recovery efficiency exceeding 85%. The regenerated FSSR-AAc can be reused for multiple adsorption cycles while retaining satisfactory adsorption performance, thus extending the service life of the biosorbent and reducing material consumption.

Second, for non-regenerable spent adsorbent, pyrolysis valorization is applicable. The Zn-loaded FSSR-AAc can be thermally converted into stable Zn-enriched biochar, which can be further utilized as a soil amendment or an immobilizing agent for heavy metals in soil remediation. In this process, zinc is stably fixed in the biochar matrix to prevent re-leaching into the environment.

These two complementary strategies realize the full-cycle resource utilization of fermented sweet sorghum stalk residues, effectively reduce secondary waste generation, and strongly align with the principles of green and sustainable development.

3.4.4. Sustainability Evaluation and Alignment with Sustainable Development Goals (SDGs)

The application of FSSR-AAc for Zn(II) removal exhibits strong sustainability and is closely associated with the United Nations Sustainable Development Goals (SDGs), supported by quantitative data and practical indicators [64].

In terms of SDG 6 (Clean Water and Sanitation), FSSR-AAc achieves a Langmuir maximum adsorption capacity of 20.98 mg/g for Zn(II), which reduces heavy metal concentrations in aqueous solutions to meet discharge standards for industrial wastewater. This efficiency ensures effective purification of zinc-contaminated water and safeguards aquatic environmental safety, providing a feasible technical solution for water pollution control.

For SDG 9 (Industry, Innovation and Infrastructure), the γ-ray irradiation grafting method enables grafting ratio of acrylic acid up to 10.2%, significantly enhancing the carboxyl content from 0.2 mmol/g in raw FSSR to 1.6 mmol/g in FSSR-AAc. This green and controllable modification technology supports the scalable production of high-performance biosorbents, promoting innovation in eco-friendly material manufacturing and industrial wastewater treatment infrastructure.

Regarding SDG 12 (Responsible Consumption and Production), the utilization of fermented sweet sorghum stalk residues realizes the valorization of agricultural waste. Approximately 1 ton of FSSR can be converted into high-efficiency biosorbent to treat thousands of liters of Zn(II)-containing wastewater. Meanwhile, the spent adsorbent can be regenerated for repeated use, or pyrolyzed into Zn-enriched biochar for soil remediation. This closed-loop utilization reduces secondary waste generation and embodies circular economy principles.

In support of SDG 13 (Climate Action), compared with petroleum-based synthetic adsorbents, FSSR-AAc reduces carbon emissions by an estimated 30–40% throughout its life cycle, as it relies on renewable biomass feedstock and energy-saving irradiation processing. The replacement of non-degradable adsorbents with waste-derived biosorbents effectively lowers the carbon footprint of water treatment and mitigates climate-related environmental burdens.

Overall, the quantitative performance indicators and environmental benefits confirm that FSSR-AAc provides a sustainable, cost-effective, and eco-friendly approach for heavy metal removal, contributing synergistically to multiple SDGs and promoting green and low-carbon development in water treatment.

4. Conclusions

In this study, a novel green biosorbent FSSR-AAc was successfully prepared via γ-ray irradiation-induced grafting of acrylic acid onto fermented sweet sorghum stalk residues, and its adsorption performance toward Zn(II) from aqueous solution was systematically investigated. The radiation grafting modification effectively introduced abundant carboxyl groups and significantly improved the adsorption capacity compared with raw FSSR. The adsorption process was well described by the Langmuir isotherm model, suggesting a monolayer chemical adsorption mechanism.

EXAFS analysis clarified that Zn(II) was adsorbed in its divalent cationic form and primarily coordinated with carboxyl groups on FSSR-AAc. The coordination number N was 4.2 and the distance between Zn-O was 1.93 Å. Cost-performance evaluation indicated that the adsorbent exhibits competitive cost and favorable scalability for large-scale applications. From a circular economy perspective, the exhausted adsorbent can be either regenerated for reuse or pyrolyzed into Zn-enriched biochar for soil remediation.

This work aligns with SDG 6 (clean water and sanitation), SDG 9 (industry, innovation and infrastructure), SDG 12 (responsible consumption and production), and SDG 13 (climate action). Overall, FSSR-AAc is a low-cost, eco-friendly, and highly efficient biosorbent with great application potential for the remediation of heavy metal-contaminated wastewater.

Author Contributions

J.W.: writing, methodology, investigation, data curation, supervision; J.D.: investigation, methodology, data curation; X.G.: data curation, software. All authors have read and agreed to the published version of the manuscript.

Funding

This research was funded by the National Key Research and Development Program (2016YFC1402507).

Institutional Review Board Statement

Not applicable.

Informed Consent Statement

Not applicable.

Data Availability Statement

The raw data used in this study can be obtained from the authors upon reasonable request. The authors will ensure the accessibility of these data to qualified professionals for at least 10 years following the publication of this paper.

Conflicts of Interest

The authors declare no conflict of interest.

Use of AI and AI-Assisted Technologies

No AI tools were utilized for this paper.

References

1. Wang, J.; Chen, C. Biosorbents for heavy metals removal and their future. *Biotechnol. Adv.* **2009**, *27*, 195–226.
2. Wang, J.; Guo, X. Adsorption kinetics and isotherm models of heavy metals by various adsorbents: An overview. *Crit. Rev. Environ. Sci. Technol.* **2023**, *53*, 1837–1865.
3. Clement, E.; Bravin, M.N.; Avadi, A.; et al. Experimental evaluation of zinc and copper terrestrial ecotoxicity prediction by life cycle assessment in agricultural recycling of livestock effluent. *Environ. Sci. Technol.* **2025**, *59*, 4122–4132.

4. Kong, J.; Guo, Q.; Wei, R.; et al. Study on the migration pathway and isotopic composition of Zn in soil, plant and water in mining area. *J. Hazard. Mater.* **2025**, *494*, 138394.
5. Yin, Y.; Wang, J. The evolution of environmental technology: From end-of-pipe to systemic solutions. *Environ. Microb. Technol.* **2026**, *1*, 1.
6. Zhai, M.; Fu, B.; Zhai, Y.; et al. Simultaneous removal of pharmaceuticals and heavy metals from aqueous phase via adsorptive strategy: A critical review. *Water Res.* **2023**, *236*, 119924.
7. Wang, J.; Wang, S. A critical review on graphitic carbon nitride ($g\text{-}C_3N_4$)-based materials: Preparation, modification and environmental application. *Coord. Chem. Rev.* **2022**, *453*, 214338.
8. Hu, H.; Zhang, J.; Wang, T.; et al. Adsorption of toxic metal ion in agricultural wastewater by torrefaction biochar from bamboo shoot shell. *J. Clean. Prod.* **2022**, *338*, 130558.
9. Huang, J.; Zhao, J.; Xu, J. Recent advance in valorization of lignocellulosic waste into biochar and its functionalization for the removal of chromium ions. *Int. J. Biol. Macromol.* **2025**, *298*, 139773.
10. Khan, Z.H.; Gao, M.; Qiu, W.; et al. Mechanisms for cadmium adsorption by magnetic biochar composites in an aqueous solution. *Chemosphere* **2020**, *246*, 125701.
11. Wang, J.; Zhuang, S. Chitosan-based materials: Preparation, modification and application. *J. Clean. Prod.* **2022**, *355*, 131825.
12. Wang, H.; Xu, J.; Liu, X.; et al. Preparation of straw activated carbon and its application in wastewater treatment: A review. *J. Clean. Prod.* **2021**, *283*, 124671.
13. Wu, J.; Dong, J.; Wang, J. Adsorptive removal of Cu(II) from aqueous solution by fermented sweet sorghum residues as a novel biosorbent. *J. Mol. Liq.* **2022**, *367*, 120362.
14. Yu, S.; Zhang, W.; Dong, X.; et al. A review on recent advances of biochar from agricultural and forestry wastes: Preparation, modification and applications in wastewater treatment. *J. Environ. Chem. Eng.* **2024**, *12*, 111638.
15. Yuan, X.; Li, S.; Yang, F.; et al. A Review on As-contaminated soil remediation using waste biomass feedstock-based biochar and metal-modified biochar. Ecotoxicol. *Environ. Saf.* **2025**, *292*, 117927.
16. Zhang, H.; Shao, J.; Zhang, S.; et al. Effect of phosphorus-modified biochars on immobilization of Cu(II), Cd(II), and As(V) in paddy soil. *J. Hazard. Mater.* **2020**, *390*, 121349.
17. Xiang, Z.; Tang, N.; Jin, X.; et al. Fabrications and applications of hemicellulose-based bio-adsorbents. *Carbohydr. Polym.* **2022**, *278*, 118945.
18. Zhao, Y.; Chen, T.; Liang, T.; et al. Efficient scavenging of Cr(VI) via radiation preparation of amino-functionalized agricultural waste loofa: Behavior and mechanism insight. *Colloids Surf. A* **2025**, *715*, 136693.
19. Liu, S.; Lou, X.; Xing, Y.; et al. Natural bioaugmentation enhances the application potential of biochar for Cd remediation. *Sep. Purif. Technol.* **2022**, *282*, 119948.
20. Zou, C.; Xu, Z.; Nie, F.; et al. Application of hydroxyapatite-modified carbonized rice husk for the adsorption of Cr(VI) from aqueous solution. *J. Mol. Liq.* **2023**, *371*, 121137.
21. Zhu, Y.; Hu, J.; Wang, J. Competitive adsorption of Pb(II), Cu(II) and Zn(II) onto xanthate-modified magnetic chitosan. *J. Hazard. Mater.* **2012**, *221*, 155–161.
22. Gao, Z.; Shang, D.; He, J.; et al. Effects and mechanism on cadmium adsorption removal by CaCl2-modified biochar from selenium-rich straw. *Bioresour. Technol.* **2023**, *370*, 128563.
23. Bhadoria, P.; Shrivastava, M.; Khandelwal, A.; et al. Preparation of modified rice straw-based bio-adsorbents for the improved removal of heavy metals from wastewater. *Sustain. Chem. Pharm.* **2022**, *29*, 100742.
24. Karimi, F.; Ayati, A.; Tanhaei, B.; et al. Removal of metal ions using a new magnetic chitosan nano-bio-adsorbent; a powerful approach in water treatment. *Environ. Res.* **2022**, *203*, 111753.
25. Dudziak, M.; Werle, S.; Marszalek, A.; et al. Comparative assessment of the biomass solar pyrolysis biochars combustion behavior and zinc Zn(II) adsorption. *Energy* **2022**, *261*, 125360.
26. Xu, B.; Wang, J. Radiation-induced modification of chitosan and applications for water and wastewater treatment. *J. Clean. Prod.* **2024**, *467*, 142924.
27. Tang, X.; Hu, G.; Chen, Z.; et al. High adsorption of Cu(II) in novel thiacalix [4]arene/acrylic polymer/diatomite fast fabricated by electron beam irradiation: Controllable microstructures, adsorption performance and mechanism. *Chem. Eng. J.* **2024**, *495*, 153090.
28. He, Y.; Mu, L.; Wang, M.; et al. Efficient removal of trace uranium from nuclear effluents using irradiation-functionalized fibrous adsorbents with very high salt tolerance. *Chem. Eng. J.* **2023**, *461*, 141978.
29. Torkaman, R.; Asadollahzadeh, M. Effectively trapping lanthanum ions with the NWPP polymeric adsorbent through gamma ray modification procedure in continuous bed column. *Sep. Purif. Technol.* **2025**, *358*, 130305.
30. Misra, N.; Rawat, S.; Goel, N.; et al. CellUSorb: A high-performance, radiation functionalized cellulose based adsorbent for Uranium (VI) remediation in ground water. *Sep. Purif. Technol.* **2023**, *322*, 124215.

31. Selambakkannu, S.; Othman, N.A.F.; Ting, T.M.; et al. Preparation and optimization of thorium selective ion imprinted nonwoven fabric grafted with poly(2-dimethylaminoethyl methacrylate) by electron beam irradiation technique. *J. Environ. Chem. Eng.* **2020**, *8*, 103737.
32. Dong, J.; Hu, J.; Wang, J. Radiation-induced grafting of sweet sorghum stalk for copper(II) removal from aqueous solution. *J. Hazard. Mater.* **2013**, *262*, 845–852.
33. Zhang, G.; Liu, F.; Zhong, S.; et al. Surpassing stoichiometric limitation for supra-multi-molar adsorption and separation of acid gases. *Nat. Commun.* **2025**, *16*, 2861.
34. Wei, S.; Zhu, J.; Chen, X.; et al. Planar chlorination engineering induced symmetry-broken single-atom site catalyst for enhanced CO_2 electroreduction. *Nat. Commun.* **2025**, *16*, 1652.
35. Chen, C.; Wang, J. Investigating the interaction mechanism between zinc and *Saccharomyces cerevisiae* using combined SEM-EDX and XAFS. *Appl. Microbiol. Biotechnol.* **2008**, *79*, 293–299.
36. Dewey, C.; Juillot, F.; Fendorf, S.; et al. Seasonal oxygenation of contaminated floodplain soil releases Zn to pore water. *Environ. Sci. Technol.* **2023**, *57*, 4841–4851.
37. Wang, L.; Han, X.; Liang, T.; et al. Cosorption of Zn(II) and chlortetracycline onto montmorillonite: pH effects and molecular investigations. *J. Hazard. Mater.* **2022**, *424*, 127368.
38. Tang, J.; Sun, G.; Feng, X.; et al. Mechanisms of Zn removal from water by amorphous geopolymer: Molecular-level insights from X-ray absorption spectroscopy, isotope fractionation and surface complexation modeling. *Chem. Eng. J.* **2023**, *477*, 147175.
39. Zhu, L.; Zhang, X.; Zhang, J.; et al. Saltwater intrusion weakens Fe-(oxyhydr) oxide-mediated (im)mobilization of Ni and Zn in redox-fluctuating soil-groundwater system. *Water Res.* **2022**, *221*, 118799.
40. Ledingham, G.J.; Custis, A.T.; Fang, Y.H.; et al. Short-term inhibition and long-term enhancement of irreversible trace metal binding to goethite in multi-metal systems. *Environ. Sci. Technol.* **2025**, *59*, 12302–12313.
41. Dupont, L.; Guillon, E.; Bouanda, J.; et al. EXAFS and XANES studies of retention of copper and lead by a lignocellulosic biomaterial. *Environ. Sci. Technol.* **2002**, *36*, 5062–5066.
42. Wang, J.; Guo, X. Adsorption isotherm models: Classification, physical meaning, application and solving method. *Chemosphere* **2020**, *258*, 127279.
43. Haykiri-Acma, H.; Yaman, S. Treating lignocellulosic biomass with dilute solutions at ambient temperature: Effects on cellulose crystallinity. *Biomass Convers. Bioref.* **2024**, *14*, 9967–9981.
44. Pokrovsky, O.S.; Pokrovski, G.S.; Gelabert, A.; et al. Speciation of Zn associated with diatoms using X-ray absorption spectroscopy. *Environ. Sci. Technol.* **2005**, *39*, 4490–4498.
45. Numako, C.; Nakai, I. XAFS analysis of coprecipitation of zinc by sulfide ions in an acidic solution. *Spectrochim. Acta Part B* **1999**, *54*, 133–141.
46. Panitlertumpai, N.; Nokbanpote, W.; Sangdee, A.; et al. Zinc and/or cadmium accumulation in *Gynura pseudochina* (L.) DC. studied *in vitro* and the effect on crude protein. *J. Mol. Struct.* **2013**, *1036*, 279–291.
47. Fomina, M.; Charnock, J.M.; Hillier, S.; et al. Zinc phosphate transformations by the *Paxillus involutus*/pine ectomycorrhizal association. *Microb. Ecol.* **2006**, *52*, 322–333.
48. Straczek, A.; Sarret, G.; Manceau, A.; et al. Zinc distribution and speciation in roots of various genotypes of tobacco exposed to Zn. *Environ. Exp. Bot.* **2008**, *63*, 80–90.
49. Parsons, J.G.; Hejazi, M.; Tiemann, K.J.; et al. An XAS study of the binding of copper(II), zinc(II), chromium(III) and chromium(VI) to hops biomass. *Microchem. J.* **2002**, *71*, 211–219.
50. Guine, V.; Spadini, L.; Sarret, G.; et al. Zinc sorption to three gram-negative bacteria: Combined titration, modeling, and EXAFS study. *Environ. Sci. Technol.* **2006**, *40*, 1806–1813.
51. Pan, G.; Zhu, M.Q. Quantum chemical and XAFS studies of zinc species in water solutions under full pH range conditions. *Abstr. Pap. Am. Chem. Soc.* **2004**, *228*, 729–735.
52. Li, W.; Pan, G.; Zhang, M.; et al. EXAFS studies on adsorption irreversibility of Zn(II) on TiO_2: Temperature dependence. *J. Colloid Interface Sci.* **2008**, *319*, 385–391.
53. Bochatay, L.; Persson, P.; Sjoberg, S. Metal ion coordination at the water-manganite (γ-MnOOH) interface: I. An EXAFS study of cadmium(II). *J. Colloid Interface Sci.* **2000**, *229*, 584–592.
54. Sia, G.B.; Vernasqui, L.G.; Consolin, N., Jr.; et al. Zinc adsorption from aqueous solution on biosorbent from urban pruning waste. *Environ. Technol.* **2022**, *43*, 728–736.
55. Ali, M.M.; Bhakta, J.N. Biosorption of zinc from aqueous solution using leaves of *Corchorus olitorius* as a low-cost biosorbent. *Water Environ. Res.* **2020**, *92*, 821–828.
56. Yilmaz, O.; Tugrul, N. Zinc adsorption from aqueous solution using lemon, orange, watermelon, melon, pineapple and banana rinds. *Water Pract. Technol.* **2022**, *17*, 318–328.
57. Celgan, D.; Karadag, A.; Karim, B.J.M.; et al. Cross-linked carboxymethyl cellulose biosorbent for zinc removal: A sustainable remediation of heavy metal-polluted waters. *Appl. Water Sci.* **2025**, *15*, 96.

58. Negi, A.; Joshi, S.; Joshi, S.K.; et al. Biosorption of zinc on functionally activated Lantana camara leaves: Equilibrium, kinetic, and thermodynamic studies. *Biomass Convers. Bioref.* **2025**, *15*, 24117–24134.
59. Aniagor, C.O.; Hussein, D.M.; Farag, S.; et al. Application of novel organic acid-modified biosorbent in the sequestration of aqueous zinc ion. *Sustain.Water Resour. Manag.* **2023**, *9*, 61.
60. Jayakumar, V.; Govindaradjane, S.; Rajamohan, N.; et al. Biosorption potential of brown algae, *Sargassum polycystum*, for the removal of toxic metals, cadmium and zinc. *Environ. Sci. Pollut. Res.* **2022**, *29*, 41909–41922.
61. Kajeiou, M.; Alem, A.; Mezghich, S.; et al. Competitive and non-competitive zinc, copper and lead biosorption from aqueous solutions onto flax fibers. *Chemosphere* **2020**, *260*, 127505.
62. Pagliaccia, B.; Carretti, E.; Severi, M.; et al. Heavy metal biosorption by Extracellular Polymeric Substances (EPS) recovered from anammox granular sludge. *J. Hazard. Mater.* **2022**, *424*, 126661.
63. Elouali, S.; Hamdan, Y.A.; Belmajdoub, M.; et al. Green chitosan extraction from *Hermetia illucens* breeding waste (prepupal cases): Characterization and bioadsorption activity. *Int. J. Biol. Macromol.* **2024**, *281*, 136449.
64. Meftah, S.; Meftah, K.; Drissi, M.; et al. Heavy metal polluted water: Effects and sustainable treatment solutions using bio-adsorbents aligned with the SDGs. *Discov. Sustain.* **2025**, *6*, 137.